Journal of Alloys and Compounds 551 (2013) 312–317

Contents lists available at SciVerse ScienceDirect

Journal of Alloys and Compounds

journal homepage: www.elsevier.com/locate/jalcom

Microstructural changes during the slow-cooling annealing of nanocrystalline SmCo 2:17 type magnets

S.A. Romero [a,b], M.F. de Campos [c,*], J.A. de Castro [c], A.J. Moreira [b], F.J.G. Landgraf [b,d]

[a] Instituto de Física da Universidade de São Paulo, São Paulo, Brazil
[b] Escola Politécnica da Universidade de São Paulo, São Paulo, Brazil
[c] PUVR - Universidade Federal Fluminense, Av. dos Trabalhadores 420, Vila Santa Cecília, Volta Redonda, RJ 27255-125, Brazil
[d] Instituto de Pesquisas Tecnológicas do Estado de São Paulo, São Paulo, Brazil

ARTICLE INFO

Article history:
Received 30 June 2012
Received in revised form 18 August 2012
Accepted 28 August 2012
Available online 23 October 2012

Keywords:
SmCo magnets
Anisotropy field
Stoner–Wohlfarth model
Heat treatment

ABSTRACT

The microstructure and magnetic properties of 2:17 type isotropic magnets were investigated. The slow cooling heat treatment (cooling at 1 °C/min from 820 to 400 °C, and isothermal treatment during 24 h) was interrupted after the temperatures of 820, 700, 600 and 500 °C and their hysteresis were measured with fields up to 9 T. The fully heat treated sample presented coercivity ($\mu_0 H$) of 3.32 T, after 24 h at 400 °C. The microstructure was investigated with SEM–FEG (Scanning Electron Microscope with Field Emission Gun) and X-ray Diffraction Rietveld analysis. The application of the Stoner–Wohlfarth–Callen–Liu–Cullen (SW–CLC) model points out exchange coupling between ferromagnetic $Sm_2(CoFe)_{17}$ nanocells and ferromagnetic $Sm(CoCu)_5$ present at the cell boundary phase. The results are interpreted with the double shell model: first-a cobalt-rich ferromagnetic $Sm(CoCu)_5$ shell originates exchange coupling and second-a copper-rich paramagnetic $Sm(CuCo)_5$ shell produces magnetic decoupling. This double shell helps to maximize coercivity and remanence. The anisotropy field of the $Sm_2(CoFe)_{17}$ cell phase was estimated in 7 T with the SW–CLC model.

1. Introduction

The manufacture of Sm_2Co_{17} type magnets includes a complex heat treatment, with the following sequence (steps (i)–(iv)): (i) solubilization at 1180–1220 °C (4 h), (ii) quenching, (iii) precipitation heat treatment at 800–850 °C (or 820 °C) for several hours (up to 7 h) and (iv) slow cooling, from 820 °C to 400 °C, at 0.7–1 °C/min [1–5]. This process involves several phase transformations, producing a nanostructure that is responsible for the excellent magnetic properties of these alloys. This nanostructure consists in nano cells of 2:17 phase – rhombohedral $(Sm)_2(CoFe)_{17}$ (SG = 166) separated by the cell boundary phase 1:5 hexagonal $Sm(CoCu)_5$ (SG = 191). These phases are crystallographically coherent. There is also a Zr-rich lamellae phase, 1:3 rhombohedral $(Sm,Zr)_1(Co,FeCu)_3$ [6] with $PuNi_3$ structure (SG = 166).

Several questions remain unanswered concerning the four steps heat treatment of the Sm–Co–Fe–Cu–Zr magnets. The fourth and final step – the slow cooling – is essential for developing high coercivities [1–9]. However, the nanostructure is already formed during the previous annealing step (iii) at 800–820 °C [1,9]. The only evident microstructural change is solute redistribution inside the phases, and nanoprobe analysis have indicated that the slow-cooling step provokes increase of copper content inside the cell boundary phase, and reduction of the copper inside the nano cells of 2:17 phase [6–9].

The microstructural changes during the last annealing steps (iii) and (iv) are re-evaluated in the present study using Rietveld analysis of X-ray Diffraction data, SEM (scanning electron microscope)–FEG (field emission gun) images, and also with modeling of the hysteresis curves with the Stoner–Wohlfarth–Callen–Liu–Cullen (SW–CLC) model [10–13], which gives relevant information concerning coercivity mechanisms. It is also employed a diffusion-based microstructural model able to make helpful predictions concerning change of chemical composition of the nanocrystalline phases along the heat treatment [14]. The slow cooling step (iv) was interrupted at the temperatures of 820, 700, 600 and 500 °C to evaluate the microstructural changes.

The Callen–Liu–Cullen (CLC) model [13] consists in a modification of the Stoner–Wohlfarth model, taking into account interactions between particles. These possible interactions maybe either exchange coupling or magnetostastic coupling. The CLC modification changes the shape of the hysteresis curve similarly to an inverse demagnetizing field [10,11].

2. Experimental

All samples have the same chemical composition $Sm_{0.104}Co_{0.60}Fe_{0.195}Cu_{0.072}Zr_{0.027}$, and consist in a commercial alloy imported from United Kingdom. The samples were encapsulated in quartz tubes under an Argon atmosphere and were

* Corresponding author.
E-mail address: mcampos@metal.eeimvr.uff.br (M.F. de Campos).

0925-8388/$ - see front matter © 2012 Elsevier B.V. All rights reserved.
http://dx.doi.org/10.1016/j.jallcom.2012.08.131

submitted to (i) a solubilization heat treatment at 1175 °C for 4 h, (ii) quenching in water, (iii) reheated up to 820 °C, remaining at this temperature for 7 h, and (iii) were then slow cooled (−1 °C/min) to 400 °C, and remaining for an additional 24 h at 400 °C. One sample was quenched after 7 h at 820 °C. The slow cooling heat treatment was interrupted in different steps, after reaching the temperatures of 700, 600 and 500 °C. This procedure originated a total of five samples. These samples will be named: (a) 820 °C, (b) 700 °C, (c) 600 °C, (d) 500 °C and (e) 400 °C 24 h.

Magnetic measurements were performed in samples with the shape of parallelepiped with the dimensions $5 \times 1 \times 1$ mm. The measurements were done with superconducting coil at fields up to 9 T, in a VSM (Vibrating Sample Magnetometer) EG&G Princeton Applied Research model 4500. All measurements were done at the room temperature.

The nanoscale microstructure was evaluated with FEG SEM (Field Emission Gun Scanning Electron Microscope) Microscope Nova NanoSEM 400 and X-ray Diffraction (XRD), used for Rietveld Analysis. The characterization by XRD was done in a Shimadzu 6000 equipment. Rietveld analysis was done with TOPAS Academic 4.1.

3. Results and discussion

The application of the Callen–Liu–Cullen (CLC) model results in a correction of the hysteresis curve, as shown in Eq. (1). This alteration of the hysteresis reminds an inverse demagnetization field [13]. This consists in a very simple formula (Eq. (1)):

$$h_{CLC} = h_{SW} + (1/d)m \quad (1)$$

where h is the reduced field, $h = H/H_A$ and $m = M/M_S$ is the reduced magnetization. H is the applied field, H_A is the anisotropy field, M is magnetization and M_S is the magnetization of saturation and $(1/d)$ is the CLC particle interaction parameter [10,11]. h_{SW} refers to the isotropic hysteresis presented by Stoner and Wohlfarth for phases with uniaxial anisotropy [15]. In previous studies, it was found that $(1/d)$ parameter is always positive [10,11], and this implies that the observed remanence was less than the half of saturation (M_S) predicted by the original SW model [15].

Fig. 1 shows the hysteresis of a fully heat treated magnet, sample 400 °C 24 h. This sample has coercive field of 33.2 kOe (μ_0H = 3.32 T), that is, the maximum allowed by an anisotropy field of 7 T for an isotropic sample. The $1/d$ CLC interaction parameter was plotted as zero in Fig. 1. The experimental result of Fig. 1 means that the nanocrystalline grains of 2:17 phase are well magnetic decoupled from each other. As above mentioned, in previous studies, the isotropic samples presented remanence equal or lower the half the saturation [10,11]. Remanence lower than half the saturation may be caused by magnetostatic coupling [16]. However, for the sample presented at Fig. 1, the remanence is a little bit above half of saturation. It seems there is some exchange coupling [17] with another phase, probably some ferromagnetic $Sm(CoCu)_5$. The reported coercivities for Sm–Co–Cu alloys are quite high [18,19], of the order of 2 T, and this high coercivity value suggests that the coupling (either magnetostatic coupling and/or exchange coupling) is quite possible between these two hard magnetic phases – 2:17 and 1:5. The anisotropy field (7 T) determined with the model is very near that found in other studies for rhombohedral 2:17 [10,11,20].

It is interesting the comparison of the hysteresis sample of Fig. 1, which follows closely the predictions of the SW model (and with also presence of some exchange coupling, as discussed), with the sample of Fig. 2, where the slow cooling was interrupted after 500 °C. In the Stoner–Wohlfarth model, the initial magnetization curve is the average between the first and fourth quadrants of the hysteresis curve [15]. This happens for the sample of Fig. 1, but not for the sample of Fig. 2. The initial magnetization curve of all other samples (Figs. 3–5) also does not correspond to this average predicted by SW for single domain particle. The explanation is that there is imperfect magnetic decoupling in the hysteresis curves of Figs. 2–5. Existence of imperfect magnetic decoupling means that the 2:17 nano-cells do not behave as a collection of single domain particles and, thus, do not follow exactly the SW predictions. Even so, the coercivity found for the sample of Fig. 2 is high – 16.8 kOe (μ_0H = 1.68 T). The initial magnetization curve of sample of Fig. 2 suggests that nano cells of 2:17 and cell boundary 1:5 are magnetic coupled and behave as whole like grains larger than the single domain particle size. The initial magnetization curve of Fig. 2 points out existence of domain wall displacement phenomena as nucleation – it should be noted that this magnet can be more easily magnetized than the sample of Fig. 1. There is experimental evidence that when the copper content is not high enough at the cell boundary phase, nucleation is the coercivity mechanism [4], as angular dependence of coercivity followed $1/\cos\theta$ Kondorskylaw (the experimental observation of this law means that domain wall displacement processes are relevant and compete with coherent rotation [21–23]). The θ angle is the angle between the applied field and the axis of easy magnetization of the crystal.

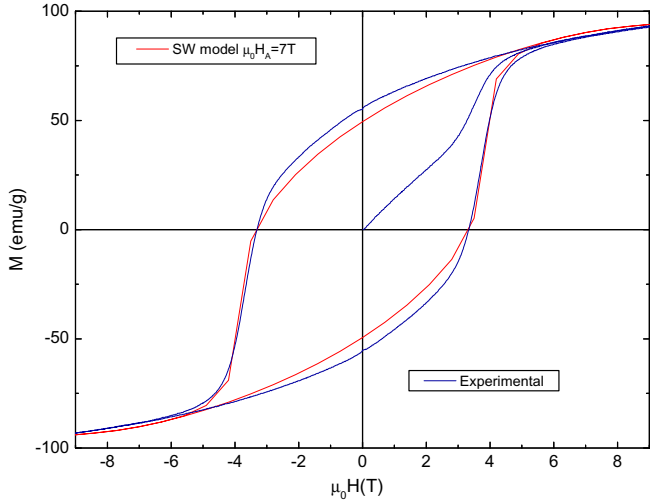

Fig. 1. Hysteresis for the sample 400 °C 24 h. Hci 33.2 kOe (μ_0Hci = 3.32T). Reduced field (H_R) = 1. The H_R parameter is defined to help the magnetic characterization of the samples. The H_R parameter is the ratio between the observed coercivity and that predicted with the SW model. The $(1/d)$ parameter was taken as null for the theoretical SW curve. The theoretical curve was plotted with μ_0H_A = 7 T.

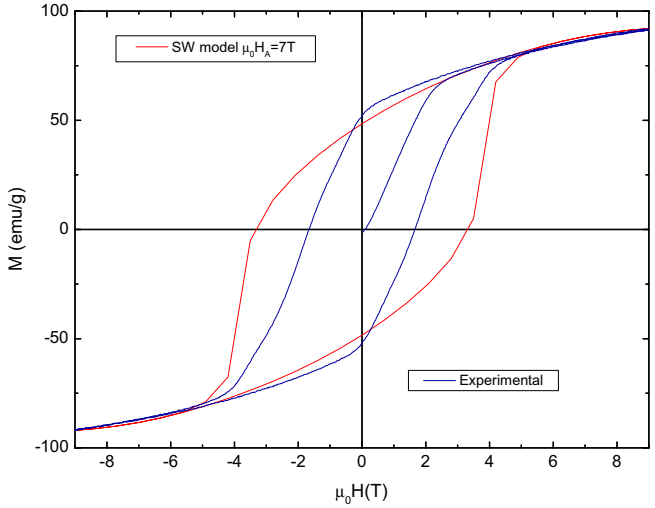

Fig. 2. Hysteresis for the sample 500 °C .Hci = 16.8 kOe (μ_0Hci = 1.68 T). Reduced field (H_R) = 16.8/33 = 0.51. The initial magnetization is not the half between the first and fourth quadrant. Thus, there is imperfect magnetic decoupling between the 2:17 nanocrystalline grains. It seems large part of cell boundary phase is ferromagnetic. The $(1/d)$ parameter was taken as null for the theoretical SW curve. The theoretical curve was plotted with μ_0H_A = 7 T.

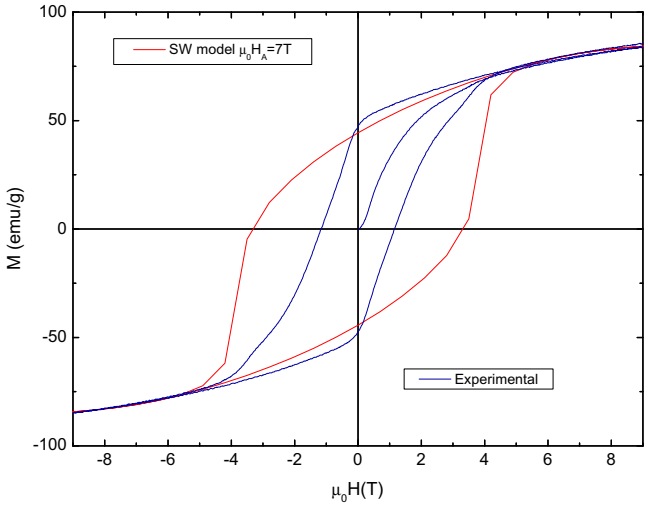

Fig. 3. Hysteresis for the sample 600 °C .Hci = 11.7 kOe (μ_0Hci = 1.17 T). Reduced field (H_R) = 11.7/33 = 0.35. Initial magnetization shows imperfect decoupling. The ($1/d$) parameter was taken as null for the theoretical SW curve. The theoretical curve was plotted with $\mu_0 H_A$ = 7 T.

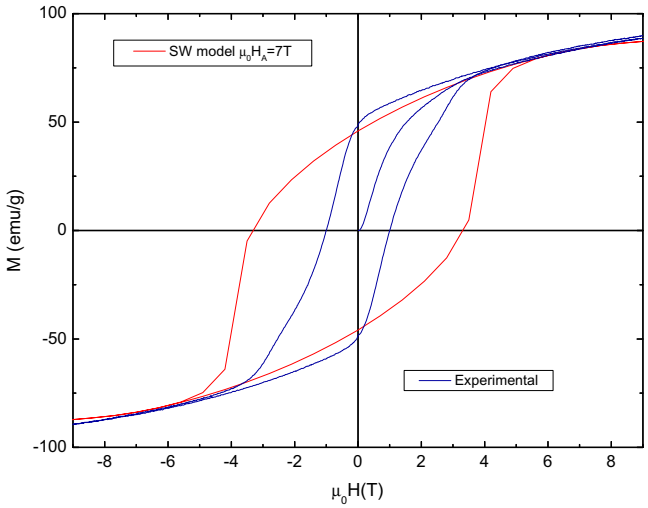

Fig. 4. Hysteresis for the sample 700 °C .Hci = 10.2 kOe (μ_0Hci = 1.02 T). Reduced field (H_R) = 10.2/33 = 0.31. The ($1/d$) parameter was taken as null for the theoretical SW curve. The theoretical curve was plotted with $\mu_0 H_A$ = 7 T.

After the comprison of Figs. 1 and 2, it is inferred that in some moment of the slow-cooling between 400 and 500 °C, a paramagnetic layer is formed inside the cell boundary phase, magnetically decoupling the 2:17 nanocrystalline cells, with significant increase of coercivity. It can be seen from Fig. 1 that the hysteresis of this magnet follows almost closely the SW behavior, and one of the main assumptions of the Stoner–Wohlfarth model is magnetically decoupled particles. It is noteworthy to add that compositions with high copper seems to have better "magnetic decoupling". Hadjipanayis and co-workers [24] found that a high copper alloy attained 20 kOe (2 T) without any slow cooling, indicating that high copper content is essential for promoting the magnetic decoupling between the 2:17 nanocells. The changes of the structure of magnetic domains observed by Gutfleisch et al. [25,26] and Fang et al. [27] along the slow cooling heat treatment strongly suggests that such magnetic decoupling happens. When the 2:17 nanograins became well magnetic decoupled, the average equilibrium distance between domain walls is reduced, as expected from magnetostatics considerations based on the domain wall theory described by Kittel [28,29].

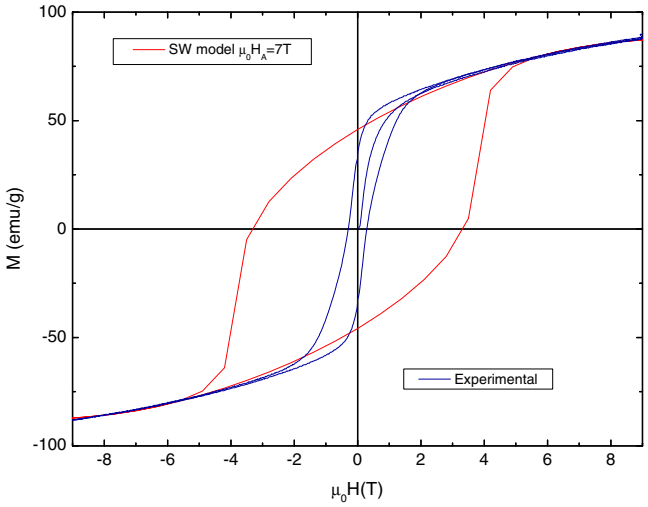

Fig. 5. Hysteresis for the sample 820 °C .Hci = 3.0 kOe (μ_0Hci = 0.3T). Reduced field (H_R) = 3.0/33 = 0.09.The ($1/d$) parameter was taken as null for the theoretical SW curve. The theoretical curve was plotted with $\mu_0 H_A$ = 7 T.

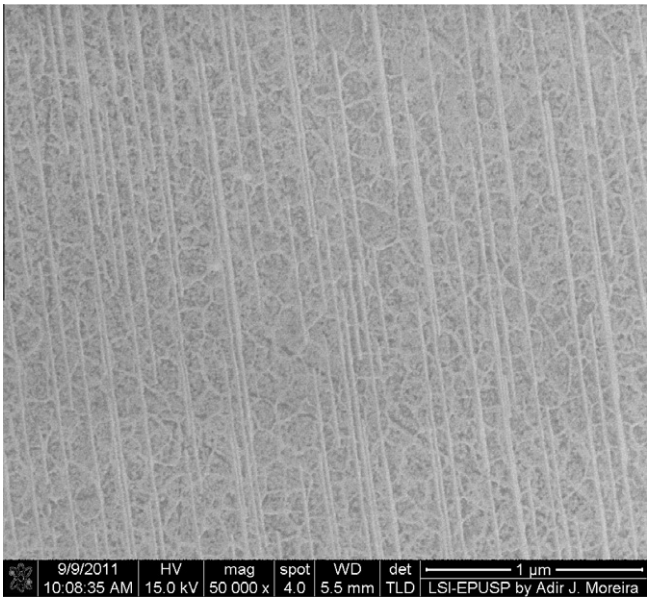

Fig. 6. SEM FEG image for sample 820 °C.

In the past, TEM (Transmission Eletron Microscopy) or HREM (High Resolution electron Microscopy) have been used for the observation of nanocells in the 2:17 magnets [3,4,6–9]. However, using TEM pictures only a very small region can be evaluated. The big advantage of the SEM–FEG technique is that large areas of the cell and cell boundary structure can be observed. The Zr-rich lamellae or platelet phase can also be observed in the SEM–FEG pictures (Figs. 6 and 7). The microstructure indicates that the nanocrystalline cells of 2:17 phase have dimensions of ~100 nm. The cell boundary thicknes is between 5–10 nm, and the volume fraction of the cell boundary phase is 5–10% (Figs. 6 and 7).

4. Microstructural model

At the step three, at temperature around 820 °C, there is a formation of nanoscale structure with $Sm_2(CoFe)_{17}$ cell phase (rhombohedral 166 structure), $Sm(CoCu)_5$ cell boundary phase

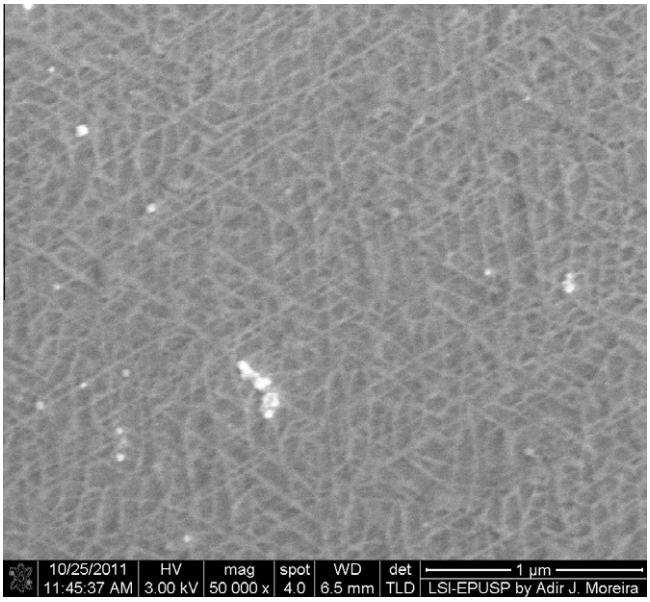

Fig. 7. SEM FEG image for sample 500 °C.

(hexagonal 191 structure) and the lamellae phase, $(ZrSm)_1(CoFeCu)_3$, see Fig. 6. The 1:3 phase has been described as Rhombohedral $Sm_1Zr_2Co_9$, a stable phase in the ternarium Sm–Zr–Co, with structure derived from $PuNi_3$ [30–32], see Table 1. The X-ray spectra of the 820 °C sample and 400 °C sample are very similar, both with ~7% of nanocrystalline $Sm(CuCu)_5$ phase (crystallite size ~12 nm), 3% of 1:3 and all the rest 2:17R (crystallite size ~50 nm provided best fitting in the Rietveld analysis). The XRD data confirms the SEM–FEG observations.

The slow cooling, as seen from Figs. 1–5, promotes very significant increase of the coercive field. The most relevant reported microstructural change is the variation of the copper content inside the cell boundary phase [6–9]. This question can be addressed by means of a diffusion model. Thus, the heat treatment kinetics can be modeled.

The copper diffusion can be modeled using Fick second law, as described in Eq. (2), which presents the three-dimension version of the Fick differential equation. The model makes use of the atomic diffusion transport equations to describe the solute redistribution. It is supposed that the main phase (2:17) is spherical, and is enveloped by a spherical shell formed by the second phase (1:5). It is assumed phase equilibrium at the interface between the particle of the main phase and the layer of the second phase. The boundary conditions at the interface are taken from the phase diagram of the system. The 2:17 nanocells are assumed to be of the 100 nm (diameter), based on the experimental data of Figs. 6 and 7. In fact, it is modelled the copper expulsion from the main magnetic phase, the nanocrystalline cells of 2:17 phase. The copper diffusion was modeled with an equation of the type $D = D_0 \exp(-Q/RT)$, using $Q = 259$ kJ/mol, and $D_0 = 10^{-4}$ m^2/s [33]. As boundary conditions, the model uses the solubility limits given by Perry [34] and assumes negligible solubility of Cu into 2:17 at 400 °C. For all other temperatures, the solubility limits were obtained from linear interpolation. The average copper content inside the 2:17 nanocrystalline cells is presented in Fig. 8, where several different slow-cooling rates were compared.

$$\frac{\partial(\mathrm{Cu})}{\partial t} = \nabla \cdot (D_{\mathrm{Cu}}(T(t))\nabla \mathrm{Cu}) \tag{2}$$

If the chemical composition of a given alloy is expressed as $Sm(Co_bCu_xFe_yZr_w)_z$, then: %at Cu = $x\ z/(z+1)$; %at Sm = $1/(z+1)$; %at Co = $b\ z/(z+1)$; %at Fe = $y\ z/(z+1)$; %at Zr = $w\ z/(z+1)$.

If we assume that 1:5 and 2:17 phases are near stoichiometric, and also considering that the Zr amount is very small, we could estimate the volume fractions of 1:5 and 2:17 phases (Vv1:5 and Vv2:17, respectively) in a quasi-binary (assuming that the densities of 1:5 and 2:17 are very similar): Vv1:5 = (% at Sm – 10.53)/6.14, and Vv2:17 = (16.67 -% at Sm)/6.14.The Eq. (3) is very important in the modeling,:

$$\%\mathrm{at\,Cu} = \mathrm{Vv1:5}(\%\mathrm{at\,Cu})1:5 + \mathrm{Vv2:17}(\%\mathrm{at\,Cu})2:17 \tag{3}$$

It has been reported that $SmCo_2Cu_3$ is paramagnetic at the room temperature [35]. Thus, if (% at Cu)1:5 >50% it is expected a magneticdecoupling effect between the 2:17 nanocells. In other words, in this case single crystals of 2:17 phase are separated by a paramagnetic 1:5 phase. Now, using Eq. (3), If the Vv1:5 is 5%, and %at Cu2:17 is reduced, for example, from 5% to 2.5% as consequence of the slow cooling heat treatment, then the %at Cu1:5 will increase 0.2375. Similarly, if Vv1:5 is 10%, then % at Cu1:5 increases 0.225.This demonstrates that the typical slow cooling heat treatment applied in a typical magnet can increase the copper in the cell boundary phase in such way that the magnetic decoupling effect takes place.

Results in the literature using nanoprobe microanalysis [6,9] are in agreement with such reduction of the copper content in the 2:17 cell phase. Zhang et al. [9] reported that the % at Cu2:17 decreased from 5% to 2–3%, in a magnet with ~5% Vv1:5, after performing slow cooling (0.5–1.0 °C/min). Xiong et al. [6] reported that the %Cu2:17 reduced from 3% to 1.5%, after a slow cooling (0.5 °C/min) from 820 °C to 520 °C.

It is very important to note that the copper content is variable inside the cell boundary phase, and it is higher at the triple junctions [3,4]. Thus, even after significant copper redistribution creating paramagnetic zones of 1:5 phase, some other 1:5 is ferromagnetic. This ferromagnetic $Sm(CoCu)_5$ is responsible for the exchange coupling effect clearly observed in Fig. 1. In fact, there are two-shells: the 2:17 nano grains are enveloped by a ferromagnetic 1:5 phase, producing increase of remanence by means of exchange coupling and by a second shell, paramagnetic, which generates magnetic decoupling effect (see Fig. 9).

Although the copper redistribution seems to be the relevant reason for the increase of coercivity, in fact there are three main reasons for the large coercivity increase along the slow-cooling annealing[14]:

(i) Formation of a $Sm(CuCo)_5$ paramagnetic phase surrounding 2:17 cells with magnetic decoupling effect.
(ii) Part of the coercivity increase should be attributed to elimination of lattice defects [36–38] like vacancies or Sm-excess atoms from the 2:17 nanocells [36]. This is the "perfect lattice hypothesis"[36–38].
(iii) Expulsion of copper from the 2:17 cells. The elimination of non-ferromagnetic solute atoms should increase the anisotropy field of the 2:17 phase in the cells.

Table 1
Structural data for the rhombohedral phase $(Sm_{0.33}Zr_{0.67})_1(TM)_3$, where TM = Co,-Cu,Fe. SG = 166. Wyckoff notation.

Atom	site	x	y	z
TM1	3b	0	0	0.5
TM2	6c	0	0	0.333
TM3	18 h	0.5	0.5	0.083
Sm	3a	0	0	0
Zr	6c	0	0	0.1414

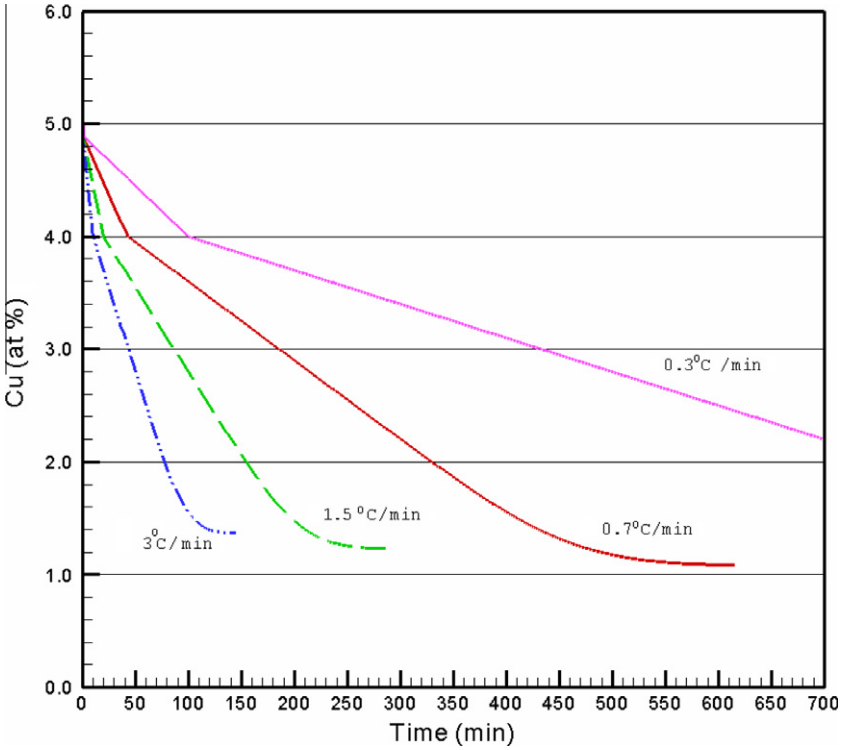

Fig. 8. Modeling copper diffusion from 2:17 phase to 1:5 cell boundary phase. The data shown in this figure is about the average copper inside the 2:17 nanograins. It was assumed diameter cell size of 100 nm. Several different slow-cooling rates were tested.

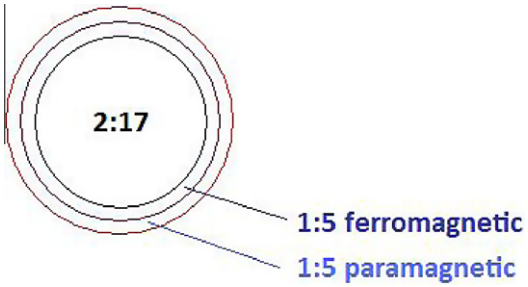

Fig. 9. The two shell layers of $Sm(Co,Cu)_5$ phase surrounding the 2:17 main ferromagnetic phase. The first layer, cobalt-rich and ferromagnetic, results in exchange coupling. The second layer, copper-rich and paramagnetic, promotes magnetic decoupling between the 2:17 nanocells. Schematic.

5. Conclusions

The great increase of coercivity along the slow-cooling of 2:17 type magnets is due to copper diffusion. This produces a paramagnetic cell boundary phase, which acts decoupling the 2:17 nanograins. If the copper content inside the cell boundary phase $Sm(CoCu)_5$ is not high enough, this effect does not happen and coercivity is low.

The application of the SW–CLC indicates clearly existence of exchange coupling between 2:17R main magnetic phase and ferromagnetic $Sm(CoCu)_5$ phase.

The results can be interpreted with the double shell model: (1) a cobalt-rich ferromagnetic $Sm(CoCu)_5$ shell originates exchange coupling and (2) a copper-rich paramagnetic Sm(CuCo) – shell produces magnetic decoupling. This "double shell" maximizes both: coercivity and remanence.

It is presented a diffusion model (based on the Fick second law). This model takes into account copper diffusion. The model is able to describe the kinetics of the phase transformations, which results in the excellent magnetic properties found in these alloys.

The structural data for 1:3R $(Sm_{0.3}Zr_{0.67})_1(CoFeCu)_3$ Space Group SG = 166 is presented. It is directly derived from $PuNi_3$ structure reported by Cromer and Olsen [32].

Acknowledgements

MF de Campos, JA de Castro, FJG Landgraf acknowledge CNPq. R N Faria for providing the SmCoFeCuZr commercial alloy used in this study. EA Perigo for assistance with XRD experiments.

References

[1] K.J. Strnat, R.M.W. Strnat, J. Magn. Magn. Mater. 100 (1991) 38–56.
[2] A.E. Ray, S. Liu, J. Mater. Eng. Perform. 1 (1992) 183.
[3] M.F. de Campos, M.M. Corte-Real, Y. Zhang, G.C. Hadjipanayis, J.F. Liu, in: N.M. Dempsey, P. de Rango (Eds.), Proceedings of the 18th International Workshop on HighPerformance Magnets and Their Applications, Annecy, France, 2004, pp. 295–301.
[4] M.M. Corte-Real, M.F. de Campos, Y. Zhang, G.C. Hadjipanayis, J.F. Liu, Phys. Status Solidi A 193 (2002) 302.
[5] K.H.J. Buschow, Permanent-Magnet Materials and Their Applications, Trans TechPublications, Uetikon-Zurich, 1998.
[6] X.Y. Xiong, T. Ohkubo, T. Koyama, K. Ohashi, Y. Tawara, K. Hono, Acta Mater. 52 (2004) 737.
[7] R. Gopalan, K. Hono, A. Yan, O. Gutfleisch, Scripta Mater. 60 (2009) 764–767.
[8] Y. Zhang, W. Tang, G.C. Hadjipanayis, C. Chen, C. Nelson, K. Krishnan, IEEE Trans. Magn. MAG.-37 (2001) 2525.
[9] Y. Zhang, W. Tang, G.C. Hadjipanayis, D. Goll, H. Kronmuller, C. Chen, C. Nelson, K. Krishnan, in: Proc. of 16th International Workshop on Rare-Earth Magnets and theirApplications, Sendai, Japan, 2000, p. 169.
[10] S.A. Romero, M.F. de Campos, H. Rechenberg, F.P. Missell, J. Magn. Magn. Mater. 320 (2008) e73.
[11] M.F. de Campos, S.A. Romero, F.J.G. Landgraf, F.P. Missell, J. Phys. Conf. Ser. 303 (2011) 012049.
[12] S.J. Collocott, J. Magn. Magn. Mater. 323 (2011) 2023.
[13] E. Callen, Y.J. Liu, J.R. Cullen, Phys. Rev. B 16 (1977) 263–270.
[14] M.F. de Campos, J.A. de Castro, Mater. Sci. Forum 660–661 (2010) 290–295.
[15] E.C. Stoner, E.P. Wohlfarth, Philos. Trans. R. Soc. London A240 (1948) 599.
[16] A.M. Gabay, G.C. Hadjipanayis, J. Appl. Phys. 101 (2007) 09K507.

[17] E.F. Kneller, R. Hawig, IEEE Trans. Magn. 27 (1991) 3588.
[18] H. Nagel, A.J. Perry, A. Menth, J. Appl. Phys. 47 (1976) 2662.
[19] A. Penton-Madrigal, E. Estevez-Rams, J.H. Espina-Hernandez, R. Lora-Serrano, M. Knobel, E.H.C.P. Sinnecker, L.A.S. de Oliveira, J.P. Sinnecker, R. Grossinger, R.S. Turtelli, J. Phys. D: Appl. Phys. 42 (2009) 125005.
[20] H. Saito, M. Takahashi, T. Wakiyama, G. Kido, H. Nakagawa, J. Magn. Magn. Mater. 82 (1989) 322–326.
[21] M.F. de Campos, Mater. Sci. Forum 530–531 (2006) 146.
[22] M.F. de Campos, J.A. de Castro, Mater. Sci. Forum 660–661 (2010) 279–283.
[23] M.F. de Campos, J.A. de Castro, in: S. Kobe, P.J. McGuinness (Eds.), Proc. 21th Int. Workshop on Rare Earth Magnets and Their Applications, Bled, Slovenia, 2010, pp. 61–63.
[24] W. Tang, Y. Zhang, G.C. Hadjipanayis, Appl. Phys. Lett. 77 (2000) 421.
[25] O. Gutfleisch, K.-H. Müller, M. Wolf, K. Khlopkov, A. Yan, R. Schäfer, T. Gemming, L. Schultz, J. Iron. Steel Res. Int. 13 (Suppl. 1) (2006) 48–59.
[26] O. Gutfleisch, K.-H. Muller, K. Khlopkov, M. Wolf, A. Yan, R. Schafer, T. Gemming, L. Schultz, Acta Mater. 54 (2006) 997–1008.
[27] Y.K. Fang, H.W. Chang, Z.H. Guo, T. Liu, X.M. Li, W. Li, W.C. Chang, B.S. Han, J. Alloys Comp. 462 (2008) 376–380.
[28] C. Kittel, Rev. Mod. Phys. 21 (1949) 541–583.
[29] C. Kittel, Phys. Rev. 70 (1946) 965–971.
[30] M.F. de Campos, A.C. Neiva, S.A. Romero, R.K. Murakami, H.R. Rechenberg, F.P. Missell, IEEE Trans. Magn. 42 (2006) 3770–3772.
[31] M.F. de Campos, R.K. Murakami, S.A. Romero, H.R. Rechenberg, F.P. Missell, J. Appl. Phys. 101 (2007) 09K101.
[32] D.T. Cromer, C.E. Olsen, Acta Cryst. 12 (1959) 689–694.
[33] MF de Campos. Mater Sci Forum. 727–728 (2012) 163–168.
[34] A.J. Perry, J. Less Common Met. 51 (1977) 153.
[35] E. Lectard, C.H. Allibert, R. Ballou, J. Appl. Phys. 75 (1994) 6277.
[36] M.F. de Campos, P.R. Rios, J. Alloys Comp. 377 (2004) 121–126.
[37] M.F. de Campos, H. Okumura, G.C. Hadjipanayis, D. Rodrigues, F.J.G. Landgraf, A.C. Neiva, S.A. Romero, F.P. Missell, J. Alloys Comp. 368 (2004) 304–307.
[38] M.F. de Campos, F.J.G. Landgraf, N.H. Saito, S.A. Romero, A.C. Neiva, F.P. Missell, E. de Morais, S. Gama, E.V. Obrucheva, B.V. Jalnin, J. Appl. Phys. 84 (1998) 368.